Letter

Structure−Activity Relationships of Styrylquinoline and Styrylquinoxaline Derivatives as α-Synuclein Imaging Probes

Kohei Nakagawa, Hiroyuki Watanabe,* Sho Kaide, and Masahiro Ono*
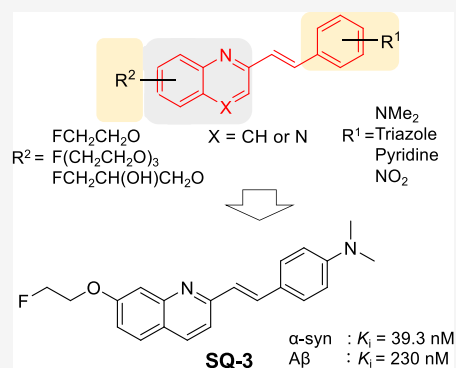
Read Online

ACCESS | Metrics & More | Article Recommendations | Supporting Information

ABSTRACT: Synucleinopathies are characterized by the deposition of α-synuclein (α-syn) aggregates before the onset of clinical symptoms. Therefore, in vivo imaging of α-syn may contribute to early diagnosis of these diseases and has attracted much attention in recent years. However, no clinically useful probes have been reported. In the present study, 16 quinoline/quinoxaline derivatives with different styryl and fluorine groups were evaluated in order to develop α-syn imaging probes. Among them, SQ3, which is a quinoline analogue with a p-(dimethylamino)styryl group and fluoroethoxy group at the 2- and 7- positions of the skeleton, displayed moderate selectivity for α-syn aggregates over β-amyloid (Aβ) aggregates (K_i = 230 nM), while maintaining high binding affinity for α-syn aggregates (K_i = 39.3 nM). In a biodistribution study, [18F]SQ3 exhibited high uptake (2.08% ID/g at 2 min after intravenous injection) into a normal mouse brain. Taken together, we demonstrate that [18F]SQ3 has basic properties as a lead compound for the development of a useful α-syn imaging probe.

R^2 =
FCH$_2$CH$_2$O
F(CH$_2$CH$_2$O)$_3$
FCH$_2$CH(OH)CH$_2$O

X = CH or N

NMe$_2$
R^1 = Triazole
Pyridine
NO$_2$

SQ-3

α-syn : K_i = 39.3 nM
Aβ : K_i = 230 nM

In recent years, with the advent of an aging society, the increase in the number of patients suffering from synucleinopathies, including Parkinson's disease, dementia with Lewy bodies, and multiple-system atrophy, has been a concern. However, even the method of definite diagnosis has not been established, let alone radical treatment. Abnormal depositions of Lewy bodies, Lewy neurites, and glial cytoplasmic inclusions are observed in the brains of patients suffering from these diseases before the onset of clinical symptoms.[1] α-Synuclein (α-syn) aggregates are major constituents of these hallmarks and have been gathering attention as biomarkers of synucleinopathies. However, the association between the progress of synucleinopathies and amount of α-syn aggregates in the brain is unclear. Therefore, in vivo imaging of α-syn is considered to contribute to early diagnosis and elucidation of the pathophysiology of synucleinopathies.

Among several imaging methods, positron emission tomography (PET) and single-photon emission computed tomography (SPECT) are excellent tools for non-invasive and quantitative imaging of biomolecules with high sensitivity. Based on this, several kinds of nuclear medicine imaging probes targeting α-syn aggregates have been reported over the past few years.[2−5] However, the detection of α-syn aggregates in vivo remains elusive. There are two major problems regarding the in vivo imaging of α-syn aggregates. The first problem is low brain permeability. Many α-syn imaging probes with high binding affinity for α-syn aggregates generally have a large molecular size (molecular weight (MW) > 430) and high lipophilicity (CLogP > 4.0), markedly decreasing brain

permeability. The second problem is selectivity for α-syn aggregates over β-amyloid (Aβ) aggregates. It is well-known that α-syn aggregates are colocalized with Aβ—which is a major biomarker of Alzheimer's disease (AD)—aggregates in some synucleinopathy patients' brains.[6] Since both proteins form aggregates with β-sheet structures, most of the probes with high affinity for α-syn aggregates also exhibit high affinity for Aβ aggregates. In addition, the concentration of α-syn aggregates is much lower than that of Aβ aggregates in the brain.[7] Taken together, α-syn imaging probes must show selectivity for α-syn aggregates versus Aβ aggregates. Therefore, it is necessary to identify a compound showing three properties: high binding affinity for α-syn aggregates, high brain uptake, and selective binding for α-syn aggregates.

Various kinds of quinoline and quinoxaline analogues were reported as amyloid imaging probes.[8−13] Some reports suggested that binding affinities for Aβ aggregates change, depending on the position of the substitution group on the quinoxaline scaffold.[11,13] Furthermore, there was a report that the quinoline scaffold with a styryl moiety at the 2-position displayed a high binding affinity for α-syn aggregates ([18F]14:

## Scheme 1. Synthesis Route of Quinoxaline Derivatives[a]
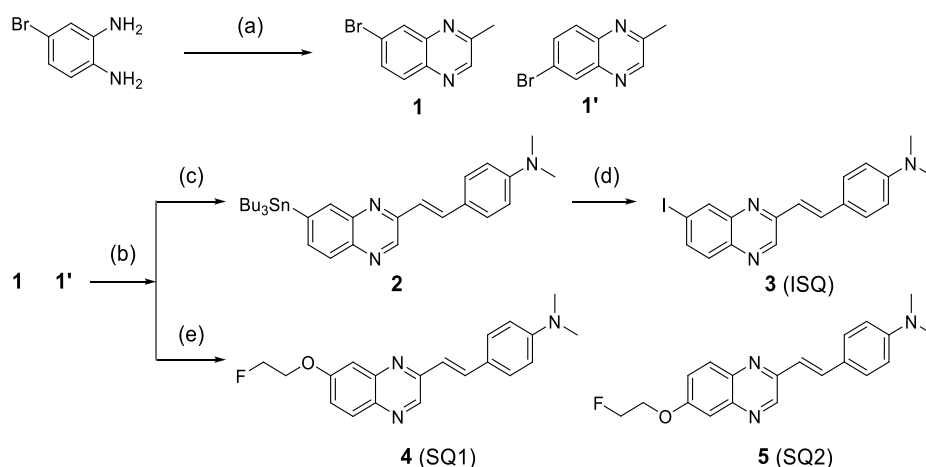
[a]Reagents and conditions: (a) pyruvic aldehyde, EtOH, 25 °C; (b) p-dimethylaminobenzaldehyde, piperidine, AcOH, toluene, reflux; (c) Bu$_4$Sn, Pd(Ph$_3$)$_4$, toluene, reflux; (d) I$_2$, CHCl$_3$, 25 °C; (e) (1) Cu(acac)$_2$, LiOH·H$_2$O, N^1,N^2-bis(4-hydroxy-2,6-dimethylphenyl)oxalamide, dimethyl sulfoxide (DMSO)/H$_2$O, 80 °C, (2) 2-fluoroethyl p-toluenesulfonate, Cs$_2$CO$_3$, DMF, 95 °C.

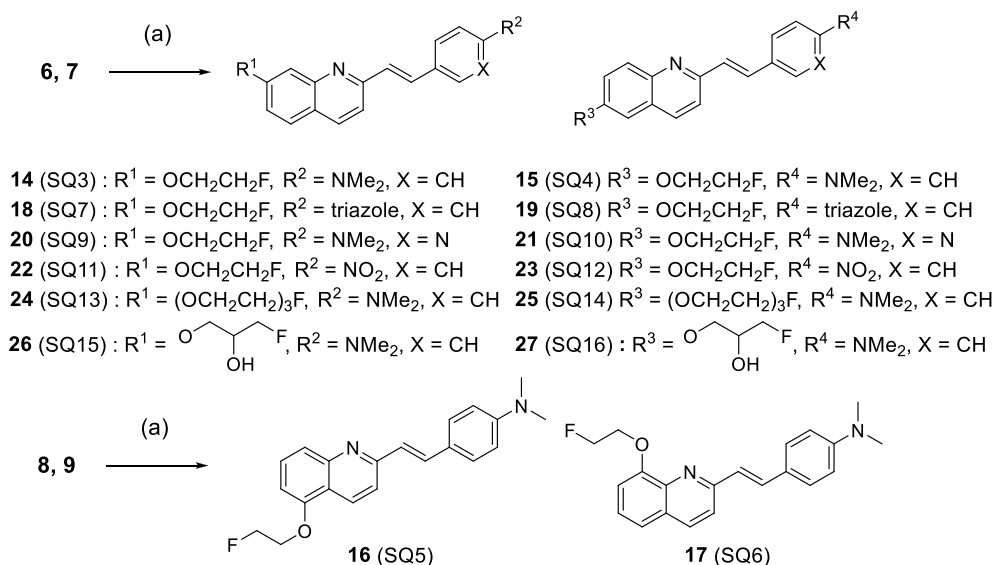## Scheme 2-1. Synthesis Routes of Quinoline, Aldehyde, and Fluorine Scaffolds[a]
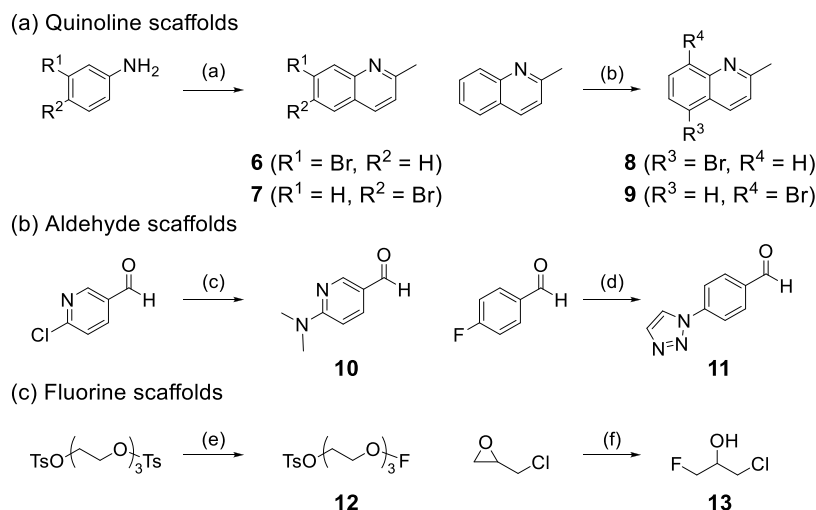
[a]Reagents and conditions: (a) ethyl vinyl ether, AcOH, 25 °C → 100 °C; (b) N-bromosuccinimide (NBS), conc. H$_2$SO$_4$, 25 °C; (c) NHMe$_2$, H$_2$O, 80 °C; (d) 1,2,3-triazole, K$_2$CO$_3$, DMF, 100 °C; (e) tetrabutylammonium fluoride (TBAF), tetrahydrofuran (THF), 70 °C; (f) TREAT HF, 130 °C.

inhibition constant K_i = 18 nM, dissociation constant K_d = 79 nM) in vitro.[14] This report also suggested that the double bond between quinoline and the aromatic ring may be important to enhance the affinity for α-syn aggregates. This study was focused on the styrylquinoline/quinoxaline backbone, and structure−activity relationship studies were performed on 16 derivatives for the development of α-syn imaging probes.
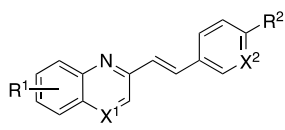
Quinoxaline derivatives were synthesized according to Scheme 1. After a mixture of 1 and 1′ was synthesized according to a method reported previously,[15] styrylquinoxaline scaffolds were obtained by a condensation reaction. In the case of 3 (ISQ), the 7-tributyltin quinoxaline scaffold was prepared from a mixture of bromo compounds using a bromo-to-tributyltin exchange reaction catalyzed by Pd(0) and isolated. Thereafter, the 7-tributyltin scaffold was reacted with I$_2$ in chloroform at 25 °C to give 3. In the case of 4 (SQ1) and 5 (SQ2), crude phenol scaffolds were reacted with 2-fluoroethyl p-toluenesulfonate in N,N-dimethylformamide (DMF) to give

4 and 5 after preparing the crude phenol scaffolds from a mixture of bromo compounds using a method reported previously.[16] Compounds 4 (SQ1) and 5 (SQ2) could be separated by column chromatography. Finally, the structures of quinoxaline derivatives were determined by X-ray crystallography. The total yields from the materials were 6−16%.

Next, quinoline derivatives were synthesized according to Schemes 2-1 and 2-2. Quinoline,[17,18] aldehyde,[19,20] and fluorine[21,22] scaffolds were synthesized using methods reported previously. Styrylquinoline scaffolds were obtained by condensation reaction from quinoline scaffolds (6, 7, 8, and 9) and aldehyde scaffolds (p-dimethylaminobenzaldehyde, p-nitrobenzaldehyde, 10, and 11). Thereafter, the phenol scaffolds were prepared from styryl scaffolds using the same method as for quinoxaline derivatives. The mixture of phenol scaffolds was reacted with fluorine scaffolds (2-fluoroethyl p-toluenesulfonate, 12, and 13) in DMF to give SQ derivatives (14−27, SQ3−16). The total yields from the materials were 0.4−17%.

Scheme 2-2. Synthesis Routes of Quinoline Derivatives[a]

14 (SQ3) : R^1 = OCH$_2$CH$_2$F, R^2 = NMe$_2$, X = CH   15 (SQ4) R^3 = OCH$_2$CH$_2$F, R^4 = NMe$_2$, X = CH

18 (SQ7) : R^1 = OCH$_2$CH$_2$F, R^2 = triazole, X = CH   19 (SQ8) R^3 = OCH$_2$CH$_2$F, R^4 = triazole, X = CH

20 (SQ9) : R^1 = OCH$_2$CH$_2$F, R^2 = NMe$_2$, X = N   21 (SQ10) R^3 = OCH$_2$CH$_2$F, R^4 = NMe$_2$, X = N

22 (SQ11) : R^1 = OCH$_2$CH$_2$F, R^2 = NO$_2$, X = CH   23 (SQ12) R^3 = OCH$_2$CH$_2$F, R^4 = NO$_2$, X = CH

24 (SQ13) : R^1 = (OCH$_2$CH$_2$)$_3$F, R^2 = NMe$_2$, X = CH   25 (SQ14) R^3 = (OCH$_2$CH$_2$)$_3$F, R^4 = NMe$_2$, X = CH

26 (SQ15) : R^1 = (O...CH$_2$...OH...F), R^2 = NMe$_2$, X = CH   27 (SQ16) : R^3 = (O...OH...F), R^4 = NMe$_2$, X = CH

16 (SQ5)   17 (SQ6)

[a]Reagents and conditions: (a) (1) aldehyde scaffolds, piperidine, AcOH, toluene, reflux, (2) Cu(acac)$_2$, LiOH·H$_2$O, N^1,N^2-bis(4-hydroxy-2,6-dimethylphenyl)oxalamide, DMSO/H$_2$O, 80 °C, (3) fluorine scaffolds, NaH or Cs$_2$CO$_3$, DMF, 95 °C.

Scheme 3. Radiosynthesis of [^{125}I]ISQ
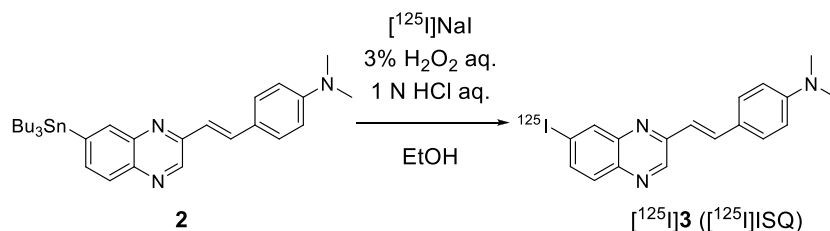
Table 1. K_i Values of SQ Derivatives for Recombinant α-Syn and Aβ Aggregates

compd	X^1	X^2	R^1	R^2	K_i (nM)[a]	
					α-syn	Aβ
SQ1	N	CH	7-OCH$_2$CH$_2$F	N(Me)$_2$	75.6 ± 43.1	83.6 ± 59.2
SQ2	N	CH	6-OCH$_2$CH$_2$F	N(Me)$_2$	11.4 ± 8.97	11.7 ± 0.97
SQ3	CH	CH	7-OCH$_2$CH$_2$F	N(Me)$_2$	39.3 ± 17.6	230 ± 49.1
SQ4	CH	CH	6-OCH$_2$CH$_2$F	N(Me)$_2$	4.38 ± 2.81	7.69 ± 0.86
SQ5	CH	CH	5-OCH$_2$CH$_2$F	N(Me)$_2$	29.2 ± 18.5	6.26 ± 3.83
SQ6	CH	CH	8-OCH$_2$CH$_2$F	N(Me)$_2$	>1000	>1000
SQ7	CH	N	7-OCH$_2$CH$_2$F	N(Me)$_2$	>1000	>1000
SQ8	CH	N	6-OCH$_2$CH$_2$F	N(Me)$_2$	56.5 ± 20.0	47.8 ± 4.84
SQ9	CH	CH	7-OCH$_2$CH$_2$F	triazole	586 ± 162	>1000
SQ10	CH	CH	6-OCH$_2$CH$_2$F	triazole	185 ± 123	21.0 ± 2.20
SQ11	CH	CH	7-OCH$_2$CH$_2$F	NO$_2$	361 ± 180	>1000
SQ12	CH	CH	6-OCH$_2$CH$_2$F	NO$_2$	275 ± 105	31.7 ± 11.3
SQ13	CH	CH	7-(OCH$_2$CH$_2$)$_3$F	N(Me)$_2$	>1000	>1000
SQ14	CH	CH	6-(OCH$_2$CH$_2$)$_3$F	N(Me)$_2$	10.8 ± 5.53	9.56 ± 1.57
SQ15	CH	CH	7-OCH$_2$CH(OH)CH$_2$F	N(Me)$_2$	618 ± 252	>1000
SQ16	CH	CH	6-OCH$_2$CH(OH)CH$_2$F	N(Me)$_2$	85.3 ± 26.1	200 ± 22.8

[a]Values are the mean ± standard deviation of the mean for 6−9 independent experiments.

The main reason for the low yields of styrylquinoline/quinoxaline derivatives was the low yields of the condensation reaction in the first step. The amount of aldehyde was increased and the reaction time was extended, but no

significant improvement in yield was observed. In addition, many inseparable byproducts were produced. Therefore, there is room for improvement in the method of this reaction.

Since ^{125}I has a longer half-life time ($T_{1/2}$ = 60 days) than [18]F ($T_{1/2}$ = 109.8 min), we used a ^{125}I-labeled compound as a competitive inhibitor. Accordingly, [^{125}I]ISQ was designed, synthesized, and evaluated. This compound is suitable as a competitive inhibitor because the structure is similar to those of the SQ derivatives. [^{125}I]ISQ was obtained from tributyltin precursor **2** by the iododestannylation reaction (Scheme 3). The radiochemical identity of the radioiodinated ligands was confirmed by co-injection with non-radioiodinated compounds from their high-performance liquid chromatography (HPLC) profiles. [^{125}I]ISQ was obtained in a radiochemical yield of 19.4% with radiochemical purities of over 95% after HPLC purification.

The affinities of ISQ were evaluated for both α-syn and Aβ aggregates. From the results of binding saturation assays using recombinant α-syn and Aβ aggregates, ISQ displayed high binding affinities for both of them (α-syn: K_d = 25.1 nM, Aβ: K_d = 8.53 nM). Considering these results, a binding inhibition assay was performed using [^{125}I]ISQ as a competitive inhibitor for both α-syn and Aβ aggregates. Table 1 summarizes the K_i value of all SQ derivatives for α-syn and Aβ aggregates.

First, four compounds (SQ1−4) were evaluated to determine which backbone (quinoline or quinoxaline) is suitable for α-syn imaging probes. A dimethylamino group was introduced in the p-position on the styryl moiety because many α-syn imaging probes with such designs have been reported.[23,24] SQ4 displayed the highest binding affinity for α-syn aggregates (K_i = 4.38 nM) of the four compounds but also bound to Aβ aggregates (K_i = 7.69 nM). SQ3 displayed moderate selectivity for α-syn aggregates over Aβ aggregates (K_i = 230 nM) while maintaining high binding affinity for α-syn aggregates (K_i = 39.3 nM). On the other hand, the fact that the quinoxaline derivatives (SQ1 and SQ2) displayed lower binding affinity for α-syn aggregates than the corresponding quinoline derivatives (SQ3 and SQ4) revealed that the quinoline backbone may be preferable to the quinoxaline backbone for α-syn imaging probes.

Next, SQ5 and SQ6 had a fluoroethoxy moiety introduced at the 5- and 8-positions of quinoline, respectively, in order to evaluate the effect of the introduction site of a substituent on binding affinities for α-syn and Aβ aggregates. Interestingly, SQ5 displayed high binding affinities for both protein aggregates (α-syn: K_i = 29.2 nM, Aβ: K_i = 6.26 nM), although SQ6 displayed low binding affinities for them (α-syn: K_i > 1000 nM, Aβ: K_i > 1000 nM). It was suggested that there is much space near the 5- and 6-positions of the quinoline skeleton at the binding site of the SQ compounds for both protein aggregates. In addition, since the space near the 7-position at the binding site for α-synuclein aggregates of the probe might be wider than that of Aβ aggregates, it is considered that SQ3 showed higher affinity for α-syn aggregates than Aβ aggregates.

SQ4, with the highest affinity for α-syn aggregates, and SQ3, with the highest selectivity for α-syn aggregates, against Aβ aggregates of 4 compounds (SQ3−6) were selected as lead compounds for further structure−activity relationship study. Next, the brain permeability of styrylquinoline derivatives was the focus. CNS MPO SCORE is an index of brain permeability that is calculated from six elements (CLogP, MW, pK_a,
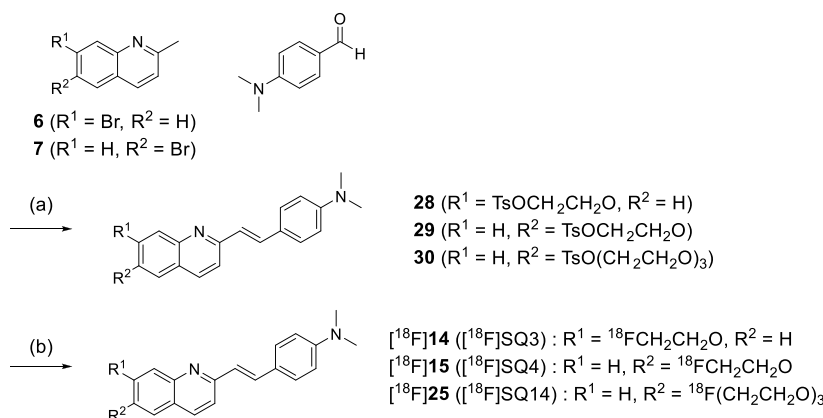
topological polar surface area (TPSA), hydrogen bond donor (HBD), and ClogD).[25] CNS MPO SCORE of most compounds showing brain permeability is equivalent to or higher than 4 (Table 2). Although SQ3 and SQ4 meet this

Table 2. MPO Score and Its Component Parameter Values

compd	CLogP	CLogD	MW	TPSA	HBD	CNS MPO score
ISQ	4.735	2.74	401.2	29.02	0	3.83
SQ1,2	4.301	2.734	337.4	38.25	0	4.77
SQ3,4	4.207	3.207	336.4	25.36	0	4.17
SQ5,6	4.207	3.207	336.4	25.36	0	4.17
SQ7,8	3.564	3.564	360.4	52.83	0	4.94
SQ9,10	3.023	2.678	337.4	38.25	0	5.32
SQ11,12	3.987	3.987	338.3	67.94	0	4.60
SQ13,14	3.924	3.481	424.5	43.82	0	4.58
SQ15,16	3.321	2.555	366.4	45.59	1	5.10

standard, six compounds (SQ7−12) were designed and evaluated with a modified styryl moiety in order to identify better α-syn imaging probes. These six compounds showed a higher MPO SCORE than SQ3 and SQ4 (Table 2). In particular, CLogP has been greatly reduced, and they were designed to improve water solubility. Moreover, it was reported that kinetics in the normal rat brain were improved by the introduction of a triazole group or pyridine ring in IMPY (*N,N*-dimethyl-4-(6-(methylthio)imixazo[1,2-*a*]-pyridinyl)aniline) derivatives, Aβ imaging probes, instead of a dimethylamine group or benzene ring.[26] It was also reported that chalcone derivatives detect α-syn aggregates with high affinity and selectivity by replacing a p-dimethylamino group with a p-nitro group.[5] However, SQ7−12 displayed lower affinity for α-syn aggregates (K_i ≥ 185 nM) than the corresponding p-dimethylamino SQ derivatives (SQ3 and SQ4). Although there are several possible causes for this result, the dimethylamino group and benzene ring are largely involved in the hydrophobic binding site of the probe for protein aggregates. For that reason, it is considered that the hydrophobic interaction would be diminished by the design to increase water solubility in order to improve brain permeability.

Next, the study focused on the fluoroethoxy moiety, and four compounds (SQ13−16) modified with this moiety in order to improve brain permeability were evaluated. These compounds also showed a higher CNS MPO SCORE than SQ3 and SQ4 (Table 2). Moreover, a previous study indicated that brain permeability was improved by the introduction of fluorotriethylene glycol or (3-fluoro-2-hydroxy)propoxy instead of a fluoroethoxy moiety.[12] However, most of them displayed lower affinity for α-syn aggregates than the corresponding fluoroethoxy SQ derivatives (SQ3 and SQ4). Only SQ14 displayed high binding affinity for α-syn aggregates (K_i = 10.8 nM) but also showed high binding affinity for Aβ aggregates (K_i = 9.56 nM). It was suggested that long linkers at the 7-position of the quinoline backbone and linkers with hydroxyl groups may reduce the binding affinity for α-syn aggregates. To summarize the results for SQ7−14, although we used CNS MPO SCORE to increase brain permeability, it is suggested that the improvement of water solubility markedly reduced the binding affinity for α-syn aggregates, as for styrylquinoline derivatives.

Scheme 4. Synthesis Route of Precursors 28, 29, and 30 and Radiosynthesis of [^{18}F]SQ3, [^{18}F]SQ4, and [^{18}F]SQ14

6 (R^1 = Br, R^2 = H)
7 (R^1 = H, R^2 = Br)

(a)

28 (R^1 = TsOCH$_2$CH$_2$O, R^2 = H)
29 (R^1 = H, R^2 = TsOCH$_2$CH$_2$O)
30 (R^1 = H, R^2 = TsO(CH$_2$CH$_2$O)$_3$)

(b)

[^{18}F]**14** ([^{18}F]SQ3) : R^1 = ^{18}FCH$_2$CH$_2$O, R^2 = H
[^{18}F]**15** ([^{18}F]SQ4) : R^1 = H, R^2 = ^{18}FCH$_2$CH$_2$O
[^{18}F]**25** ([^{18}F]SQ14) : R^1 = H, R^2 = ^{18}F(CH$_2$CH$_2$O)$_3$

^{a}Reagents and conditions: (a) (1) quinoline scaffolds (**6** or **7**), piperidine, AcOH, toluene, reflux, (2) Cu(acac)$_2$, LiOH·H$_2$O, N^1,N^2-bis(4-hydroxy-2,6-dimethylphenyl)oxalamide, DMSO/H$_2$O, 80 °C, (3) tosyl scaffolds (1,2-bis(tosyloxy)ethane or triethylene glycol bis(p-toluenesulfonate), Cs$_2$CO$_3$, DMF, 100 °C; (b) Kryptofix 222, [^{18}F]KF, DMF, 120 °C.

Summarizing the results of SQ1−14, SQ3 had the highest selectivity for α-syn aggregates against Aβ aggregates. Efficacious α-syn imaging agents show K_i ≤ 1 nM for α-syn,[27] although it is not possible to establish a clear standard because the quantitative value varies greatly depending on the kind of inhibitor in the inhibition assay. In addition, since α-syn aggregates have a lower concentration in the brain than Aβ aggregates and the size of the aggregates is smaller, the selectivity against Aβ aggregates should be 10 times higher or more. Considering the results from these points of view, the binding affinity and selectivity versus Aβ aggregates of SQ3 are considered to be moderate.

CNS MPO SCORE is only a predictive index, and there is no correlation between CNS MPO SCORE and brain uptake for some compounds. From the results of the binding assay, both SQ4 and SQ14 showed much higher affinity for α-syn aggregates than SQ3. Therefore, three compounds (SQ3, SQ4, and SQ14) were labeled with ^{18}F to evaluate brain uptake and the correlation between brain uptake and CNS MPO SCORE. The tosyl precursors (**28**, **29**, and **30**) of [^{18}F]SQ3, [^{18}F]SQ4, and [^{18}F]SQ14 were prepared using the same method as for non-radioactive SQ3 (Scheme 4). [^{18}F]SQ3, [^{18}F]SQ4, and [^{18}F]SQ14 were obtained from **28**, **29**, and **30** by a nucleophilic substitution reaction. The radiochemical identity of the radiofluorinated ligands was confirmed by the same method of ^{125}I radiolabeling. [^{18}F]SQ3, [^{18}F]SQ4, and [^{18}F]SQ14 were obtained in radiochemical yields of 20.0, 30.2, and 2.2%, respectively, with radiochemical purities of over 99% after HPLC purification. Specific activities of [^{18}F]SQ3, [^{18}F]SQ4, and [^{18}F]SQ14 were 4260, 23.4, and 298 MBq/mmol, respectively.

To evaluate brain uptake and washout, a biodistribution experiment using normal mice was performed (Table 3). In order to specifically detect α-syn aggregates in the brain, it is desirable for α-syn imaging probes to be rapidly taken up at an early time-point after injection and rapidly washed out from the brain because normal mice do not have α-syn aggregates in the brain. The radioactivity accumulation of [^{18}F]SQ3, [^{18}F]SQ4, and [^{18}F]SQ14 in the brain was 2.08, 1.78, and 2.57 percentage injected dose per gram (% ID/g) at 2 min post injection, respectively. There was a positive correlation between CNS MPO SCORE and brain uptake. Thereafter, it was dispersed with time, decreasing to 1.05−1.58 and 0.93−

1.13% ID/g at 30 and 60 min post injection, respectively. These uptakes were higher than those with [^{18}F]2FBox[3] (0.47% ID/g peak at 12 min after intravenous injection), which detected α-syn aggregates in an *ex vivo* autoradiography study, and [$^{123/125}$I]PHNP-3[5] (0.78% ID/g peak at 2 min after intravenous injection), which detected α-syn aggregates selectively in fluorescence staining. However, these values were lower than those of Aβ and tau probes, which are used clinically.[28,29] Washout from the brain was confirmed for all compounds (Figure 1). However, the radioactivity accumulation after 60 min exceeded 1% ID/g for all compounds, indicating that a part of these compounds tended to remain in the brain. The difference between SQ3 and SQ4 was not clear, but it is predicted that the difference in metabolic rate may have led to the difference in washout.

Marked accumulation of [^{18}F]SQ3 and [^{18}F]SQ4 in the bone was not observed (1.67, 1.45 and 2.56, 3.36% ID/g at 2 and 60 min post injection, respectively), indicating that they may exhibit high stability against defluorination *in vivo* until 60 min post injection. On the other hand, defluorination of [^{18}F]SQ14 with fluorotriethylene glycol was observed (2.44 and 7.48% ID/g at 2 and 60 min post injection, respectively).

Based on these results, [^{18}F]SQ3 also exhibited the most favorable pharmacokinetics in terms of brain permeability and stability against defluorination. In addition, considering the results of SQ4 and SQ14, a compound design which reduces lipophilicity while maintaining the molecular size is needed to achieve more favorable brain pharmacokinetics than with SQ3. However, from a clinical point of view, there are still points to be improved regarding the slow clearance rate and moderate brain permeability.

Sixteen styrylquinoline/quinoxaline derivatives were newly designed, synthesized, and evaluated to identify a novel *in vivo* α-syn imaging probe. This study revealed that a quinoline backbone is more preferable than a quinoxaline backbone in light of binding affinity for α-syn aggregates. In addition, binding affinities for both α-syn and Aβ aggregates changed markedly depending on both the sites and kinds of substituent. In particular, SQ3, with a fluoroethoxy group at the 7-position, showed good binding affinity for α-syn aggregates and moderate selectivity for α-syn aggregates over Aβ aggregates *in vitro* among these compounds. Moreover, [^{18}F]SQ3 also exhibited favorable brain pharmacokinetics in normal mice.

Table 3. Biodistribution of Radioactivity after Intravenous Injection of [¹⁸F]SQ3, [¹⁸F]SQ4, and [¹⁸F]SQ14 in Normal Mice[a]

	time after injection (min)			
tissue	2	10	30	60
	[¹⁸F]SQ3			
blood	4.04 (0.40)	2.29 (0.53)	1.97 (0.31)	1.97 (0.22)
liver	16.07 (2.37)	16.51 (1.60)	11.26 (1.23)	7.83 (0.86)
kidney	10.41 (0.59)	7.87 (0.87)	5.51 (0.68)	4.19 (0.46)
intestine	2.08 (0.44)	3.81 (0.38)	7.97 (0.93)	10.22 (2.07)
spleen	2.47 (0.29)	2.70 (0.29)	2.29 (0.25)	1.79 (0.62)
pancreas	4.57 (0.58)	3.25 (0.45)	2.32 (0.27)	1.94 (0.23)
heart	6.98 (1.09)	3.37 (0.37)	2.56 (0.30)	2.21 (0.33)
lung	6.55 (1.14)	3.86 (0.49)	2.83 (0.41)	2.29 (0.44)
stomach[b]	1.00 (0.16)	2.26 (0.28)	3.38 (0.84)	4.22 (0.93)
brain	2.08 (0.17)	1.94 (0.30)	1.58 (0.27)	1.13 (0.13)
bone	1.67 (0.51)	2.11 (0.55)	2.36 (0.64)	2.56 (0.52)
	[¹⁸F]SQ4			
blood	10.93 (1.50)	4.34 (0.49)	2.16 (0.74)	1.55 (0.11)
liver	19.72 (2.48)	35.82 (3.71)	34.00 (4.63)	31.57 (4.21)
kidney	13.17 (1.59)	16.62 (2.63)	13.12 (2.67)	11.57 (2.30)
intestine	1.98 (0.44)	3.39 (0.29)	4.92 (0.94)	7.69 (0.65)
spleen	2.99 (0.53)	5.65 (1.02)	5.13 (1.19)	4.97 (1.19)
pancreas	2.93 (0.84)	2.31 (0.24)	1.84 (0.45)	2.06 (0.60)
heart	6.33 (1.21)	3.10 (1.68)	2.54 (0.23)	2.03 (1.05)
lung	10.15 (0.59)	6.78 (0.78)	4.11 (0.74)	3.49 (0.73)
stomach[b]	1.50 (0.39)	2.70 (0.78)	3.11 (1.51)	3.89 (1.10)
brain	1.78 (0.64)	1.28 (0.17)	1.05 (0.52)	0.93 (0.09)
bone	1.45 (0.29)	1.48 (0.35)	2.08 (0.68)	3.36 (0.84)
	[¹⁸F]SQ14			
blood	5.88 (2.31)	2.51 (0.78)	1.89 (0.13)	1.80 (0.30)
liver	9.67 (0.80)	15.08 (3.08)	13.23 (1.41)	12.92 (2.31)
kidney	12.91 (1.35)	11.89 (2.00)	7.71 (0.82)	6.80 (2.14)
intestine	2.40 (0.40)	3.40 (0.79)	7.43 (0.91)	10.11 (1.90)
spleen	2.94 (0.36)	3.49 (0.66)	2.40 (0.31)	1.96 (0.47)
pancreas	3.85 (0.77)	2.63 (0.35)	1.80 (0.18)	1.39 (0.08)
heart	5.55 (0.61)	3.22 (0.31)	2.23 (0.17)	1.97 (0.35)
lung	6.44 (0.96)	3.73 (0.83)	2.63 (0.16)	2.35 (0.34)
stomach[b]	1.10 (0.14)	2.01 (0.32)	3.14 (0.64)	3.04 (0.64)
brain	2.57 (0.70)	2.02 (0.23)	1.40 (0.22)	0.93 (0.16)
bone	2.44 (0.50)	6.35 (3.52)	6.76 (1.40)	7.48 (2.36)

[a]Expressed as % injected dose per gram. Each value represents the mean (SD) of 5 animals. [b]Expressed as % injected dose per organ.
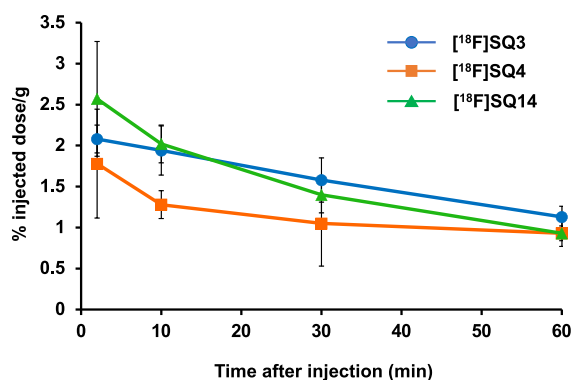

Figure 1. Washout from brains of normal mice of each compound ([¹⁸F]SQ3, [¹⁸F]SQ4, and [¹⁸F]SQ14).

These encouraging *in vitro* and *in vivo* results suggest that [¹⁸F]SQ3 has basic properties as a lead compound for the development of a useful α-syn imaging probe.

ASSOCIATED CONTENT

SI **Supporting Information**

The Supporting Information is available free of charge at https://pubs.acs.org/doi/10.1021/acsmedchemlett.2c00279.

Full experiments methods and ¹H and ¹³C NMR spectra (PDF)

AUTHOR INFORMATION

Corresponding Authors

Hiroyuki Watanabe − *Department of Patho-Functional Bioanalysis, Graduate School of Pharmaceutical Sciences, Kyoto University, Kyoto 606-8501, Japan;* ● orcid.org/ 0000-0002-8873-1224; Phone: +81-75-753-4566; Email: hwatanabe@pharm.kyoto-u.ac.jp; Fax: +81-75-753-4568

Masahiro Ono − *Department of Patho-Functional Bioanalysis, Graduate School of Pharmaceutical Sciences, Kyoto*

University, Kyoto 606-8501, Japan; ● orcid.org/0000-0002-2497-039X; Email: ono@pharm.kyoto-u.ac.jp

Authors

Kohei Nakagawa − *Department of Patho-Functional Bioanalysis, Graduate School of Pharmaceutical Sciences, Kyoto University, Kyoto 606-8501, Japan*

Sho Kaide − *Department of Patho-Functional Bioanalysis, Graduate School of Pharmaceutical Sciences, Kyoto University, Kyoto 606-8501, Japan*

Complete contact information is available at:
https://pubs.acs.org/10.1021/acsmedchemlett.2c00279

Notes

The authors declare no competing financial interest.

■ ABBREVIATIONS

α-syn, α-synuclein; AD, Alzheimer's disease; Aβ, β-amyloid; DMF, *N*,*N*-dimethylformamide; DMSO, dimethyl sulfoxide; HBD, hydrogen bond donor; HPLC, high-performance liquid chromatography; MW, molecular weight; NBS, *N*-bromosuccinimide; %ID/g, percentage injected dose per gram; PET, positron emission tomography; SPECT, single-photon emission computed tomography; TBAF, tetrabutylammonium fluoride; THF, tetrahydrofuran; TPSA, topological polar surface area

■ REFERENCES

(1) Goedert, M.; Jakes, R.; Spillantini, M. G. The Synucleinopathies: Twenty Years On. *J. Parkinsons Dis.* **2017**, *7* (s1), S51−S69.

(2) Kuebler, L.; Buss, S.; Leonov, A.; Ryazanov, S.; Schmidt, F.; Maurer, A.; Weckbecker, D.; Landau, A. M.; Lillethorup, T. P.; Bleher, D.; Saw, R. S.; Pichler, B. J.; Griesinger, C.; Giese, A.; Herfert, K. [¹¹C]MODAG-001-towards a PET tracer targeting α-synuclein aggregates. *Eur. J. Nucl. Med. Mol. Imaging* **2021**, *48* (6), 1759−1772.

(3) Verdurand, M.; Levigoureux, E.; Zeinyeh, W.; Berthier, L.; Mendjel-Herda, M.; Cadarossanesaib, F.; Bouillot, C.; Iecker, T.; Terreux, R.; Lancelot, S.; Chauveau, F.; Billard, T.; Zimmer, L. In Silico, in Vitro, and in Vivo Evaluation of New Candidates for alpha-Synuclein PET Imaging. *Mol. Pharmaceutics* **2018**, *15* (8), 3153−3166.

(4) Miranda-Azpiazu, P.; Svedberg, M.; Higuchi, M.; Ono, M.; Jia, Z.; Sunnemark, D.; Elmore, C. S.; Schou, M.; Varrone, A. Identification and in vitro characterization of C05−01, a PBB3 derivative with improved affinity for α-synuclein. *Brain Res.* **2020**, *1749*, 147131.

(5) Kaide, S.; Watanabe, H.; Iikuni, S.; Hasegawa, M.; Itoh, K.; Ono, M. Chalcone Analogue as New Candidate for Selective Detection of α-Synuclein Pathology. *ACS Chem. Neurosci.* **2022**, *13* (1), 16−26.

(6) Kotzbauer, P. T.; Cairns, N. J.; Campbell, M. C.; Willis, A. W.; Racette, B. A.; Tabbal, S. D.; Perlmutter, J. S. Pathologic accumulation of α-synuclein and Aβ in Parkinson disease patients with dementia. *Arch Neurol.* **2012**, *69* (10), 1326−1331.

(7) Eberling, J. L.; Dave, K. D.; Frasier, M. A. α-synuclein imaging: a critical need for Parkinson's disease research. *J. Parkinsons Dis.* **2013**, *3* (4), 565−567.

(8) Fodero-Tavoletti, M. T.; Okamura, N.; Furumoto, S.; Mulligan, R. S.; Connor, A. R.; McLean, C. A.; Cao, D.; Rigopoulos, A.; Cartwright, G. A.; O'Keefe, G.; Gong, S.; Adlard, P. A.; Barnham, K. J.; Rowe, C. C.; Masters, C. L.; Kudo, Y.; Cappai, R.; Yanai, K.; Villemagne, V. L. ¹⁸F-THK523: a novel in vivo tau imaging ligand for Alzheimer's disease. *Brain* **2011**, *134* (4), 1089−1100.

(9) Yang, Y.; Jia, H. M.; Liu, B. L. (E)-5-styryl-1H-indole and (E)-6-styrylquinoline derivatives serve as probes for β-amyloid plaques. *Molecules* **2012**, *17* (4), 4252−4265.

(10) Cui, M.; Ono, M.; Kimura, H.; Liu, B.; Saji, H. Novel quinoxaline derivatives for in vivo imaging of β-amyloid plaques in the brain. *Bioorg. Med. Chem. Lett.* **2011**, *21* (14), 4193−4196.

(11) Yoshimura, M.; Ono, M.; Matsumura, K.; Watanabe, H.; Kimura, H.; Cui, M.; Nakamoto, Y.; Togashi, K.; Okamoto, Y.; Ihara, M.; Takahashi, R.; Saji, H. Structure-Activity Relationships and in Vivo Evaluation of Quinoxaline Derivatives for PET Imaging of β-Amyloid Plaques. *ACS Med. Chem. Lett.* **2013**, *4* (7), 596−600.

(12) Tago, T.; Furumoto, S.; Okamura, N.; Harada, R.; Adachi, H.; Ishikawa, Y.; Yanai, K.; Iwata, R.; Kudo, Y. Structure-Activity Relationship of 2-Arylquinolines as PET Imaging Tracers for Tau Pathology in Alzheimer Disease. *J. Nucl. Med.* **2016**, *57* (4), 608−614.

(13) Zhou, K.; Yang, F.; Li, Y.; Chen, Y.; Zhang, X.; Zhang, J.; Wang, J.; Dai, J.; Cai, L.; Cui, M. Synthesis and Evaluation of Fluorine-18 Labeled 2-Phenylquinoxaline Derivatives as Potential Tau Imaging Agents. *Mol. Pharmaceutics* **2021**, *18* (3), 1176−1195.

(14) Yue, X.; Dhavale, D. D.; Li, J.; Luo, Z.; Liu, J.; Yang, H.; Mach, R. H.; Kotzbauer, P. T.; Tu, Z. Design, synthesis, and in vitro evaluation of quinolinyl analogues for α-synuclein aggregation. *Bioorg. Med. Chem. Lett.* **2018**, *28* (6), 1011−1019.

(15) Bürli, R.; et al. Fused pyrazine derivatives as kinase inhibitors. WO2010052448A2, 2010.

(16) Xia, S.; Gan, L.; Wang, K.; Li, Z.; Ma, D. Copper-Catalyzed Hydroxylation of (Hetero)aryl Halides under Mild Conditions. *J. Am. Chem. Soc.* **2016**, *138* (41), 13493−13496.

(17) Chandrashekarappa, K. K. H.; Mahadevan, K. M.; Manjappa, K. B. High throughput one pot synthesis of 2-methylquinolines. *Tetrahedron Lett.* **2013**, *54* (11), 1368−1370.

(18) Eros, G.; Nagy, K.; Mehdi, H.; Papai, I.; Nagy, P.; Kiraly, P.; Tarkanyi, G.; Soos, T. Catalytic hydrogenation with frustrated Lewis pairs: selectivity achieved by size-exclusion design of Lewis acids. *Chemistry.* **2012**, *18* (2), 574−585.

(19) Zhou, K.; Bai, H.; Feng, L.; Dai, J.; Cui, M. Smart D-π-A Type Near-Infrared Abeta Probes: Effects of a Marked pi Bridge on Optical and Biological Properties. *Anal. Chem.* **2017**, *89* (17), 9432−9437.

(20) Turner, W. W. Hepatitis B core protein allosteric modulators. WO2015138895A1, 2015.

(21) Moldovan, R. P.; Teodoro, R.; Gao, Y.; Deuther-Conrad, W.; Kranz, M.; Wang, Y.; Kuwabara, H.; Nakano, M.; Valentine, H.; Fischer, S.; Pomper, M. G.; Wong, D. F.; Dannals, R. F.; Brust, P.; Horti, A. G. Development of a High-Affinity PET Radioligand for Imaging Cannabinoid Subtype 2 Receptor. *J. Med. Chem.* **2016**, *59* (17), 7840−7855.

(22) Chaabouni, M. M.; Baklouti, A. Ring-Cleavage Reactions of F-Alkyl and Cl-Alkyl Epoxides by Action of Amines Hydrofluorides. *Bull. Soc. Chim. Fr.* **1989**, No. 4, 549−553.

(23) Ono, M.; Doi, Y.; Watanabe, H.; Ihara, M.; Ozaki, A.; Saji, H. Structure−activity relationships of radioiodinated diphenyl derivatives with different conjugated double bonds as ligands for α-synuclein aggregates. *RSC Adv.* **2016**, *6*, 44305−44312.

(24) Fodero-Tavoletti, M. T.; Mulligan, R. S.; Okamura, N.; Furumoto, S.; Rowe, C. C.; Kudo, Y.; Masters, C. L.; Cappai, R.; Yanai, K.; Villemagne, V. L. In vitro characterisation of BF227 binding to α-synuclein/Lewy bodies. *Eur. J. Pharmacol.* **2009**, *617* (1−3), 54−58.

(25) Zhang, L.; Villalobos, A.; Beck, E. M.; Bocan, T.; Chappie, T. A.; Chen, L.; Grimwood, S.; Heck, S. D.; Helal, C. J.; Hou, X.; Humphrey, J. M.; Lu, J.; Skaddan, M. B.; McCarthy, T. J.; Verhoest, P. R.; Wager, T. T.; Zasadny, K. Design and selection parameters to accelerate the discovery of novel central nervous system positron emission tomography (PET) ligands and their application in the development of a novel phosphodiesterase 2A PET ligand. *J. Med. Chem.* **2013**, *56* (11), 4568−4579.

(26) Okumura, Y.; Maya, Y.; Onishi, T.; Shoyama, Y.; Izawa, A.; Nakamura, D.; Tanifuji, S.; Tanaka, A.; Arano, Y.; Matsumoto, H. Design, Synthesis, and Preliminary Evaluation of SPECT Probes for Imaging β-Amyloid in Alzheimer's Disease Affected Brain. *ACS Chem. Neurosci.* **2018**, *9* (6), 1503−1514.

(27) Korat, Š.; Bidesi, N. S.; Bonanno, F.; Di Nanni, A.; Hoàng, A. N.; Herfert, K.; Maurer, A.; Battisti, U. M.; Bowden, G. D.; Thonon, D.; Vugts, D.; Windhorst, A. D.; Herth, M. M. α-Synuclein PET Tracer Development-An Overview about Current Efforts. *Pharmaceuticals (Basel).* **2021**, *14* (9), 847.

(28) Snellman, A.; Rokka, J.; Lopez-Picon, F. R.; Eskola, O.; Wilson, I.; Farrar, G.; Scheinin, M.; Solin, O.; Rinne, J. O.; Haaparanta-Solin, M. Pharmacokinetics of [^{18}F]flutemetamol in wild-type rodents and its binding to β amyloid deposits in a mouse model of Alzheimer's disease. *Eur. J. Nucl. Med. Mol. Imaging.* **2012**, *39* (11), 1784−1795.

(29) Xia, C. F.; Arteaga, J.; Chen, G.; Gangadharmath, U.; Gomez, L. F.; Kasi, D.; Lam, C.; Liang, Q.; Liu, C.; Mocharla, V. P.; Mu, F.; Sinha, A.; Su, H.; Szardenings, A. K.; Walsh, J. C.; Wang, E.; Yu, C.; Zhang, W.; Zhao, T.; Kolb, H. C. [^{18}F]T807, a novel tau positron emission tomography imaging agent for Alzheimer's disease. *Alzheimers Dement.* **2013**, *9* (6), 666−676.